PAPER

Reactive metal-organic interfaces studied with hard x-ray photoelectron spectroscopy: controlled formation of metalloporphyrin interphase layers during metal vapor deposition onto porphyrin films

IOP Publishing Journal of Physics: Condensed Matter
J. Phys.: Condens. Matter **31** (2019) 094002 (10pp) https://doi.org/10.1088/1361-648X/aafa2b

Reactive metal-organic interfaces studied with hard x-ray photoelectron spectroscopy: controlled formation of metalloporphyrin interphase layers during metal vapor deposition onto porphyrin films

Martin Schmid[1], Stefan R Kachel, Benedikt P Klein, Nicolas Bock, Philipp Müller, René Riedel, Norbert Hampp and J Michael Gottfried

Philipps-Universität Marburg, Fachbereich Chemie, Hans-Meerwein-Str. 4, 35032 Marburg, Germany

E-mail: schmidm5@staff.uni-marburg.de

Received 24 September 2018, revised 9 December 2018
Accepted for publication 20 December 2018
Published 18 January 2019

Abstract

Interfaces between organic semiconductors and metallic layers are ubiquitous in organic (opto-) electronic devices and can significantly influence their functionality. Here, we studied *in situ* prepared metal-organic interfaces, which were obtained by vapor deposition of metals (Co, Fe) onto organic semiconductor films (2H-tetraphenylporphyrin), with hard x-ray photoelectron spectroscopy. In these systems, the inter*phase* zones, which are formed by diffusion and reaction of the metal in the organic material, can be clearly distinguished spectroscopically from the unreacted organic bulk, since they comprise the corresponding metalloporphyrins, CoTPP and FeTPP. In order to gain control over the thickness of the interphase layers, we varied process parameters such as sample temperature and metal-atom flux during interface preparation. We found that the temperature of the organic film during metal deposition was the only parameter that significantly influenced the formation of the interphase layers: their thicknesses were typically ~0.5 nm for deposition at 90 K, compared to ~1 nm at 300 K, irrespective of metal atom flux and chemical nature of the metal atom (Fe versus Co). Notably, these values are significantly smaller than the thicknesses of other metal/organics interphase regions reported in the literature.

Keywords: metal-organic interphase, HAXPES, internal interface, metalation reaction of porphyrins

(Some figures may appear in colour only in the online journal)

1. Introduction

In organic electronic devices, interfaces between organic (semiconducting) materials and metal electrodes play a decisive role [1, 2], because the transport of charge carriers across these interfaces often limits the performance of a device [3–5]. The charge injection efficiency at the interface can be influenced by an interlayer between the metal and the organic semiconductor. For example, it has been demonstrated that an ultrathin vanadium oxide (VO_x) interlayer at the Cu/pentacene interface leads to a reduced contact resistance and an enhanced performance in organic field-effect transistors. Similar findings were reported for Au/VO_x/pentacene and Au/VO_x/BOPAnt systems [6]. Such performance-modifying interlayers can also be formed spontaneously when interdiffusion and reaction between the metal and the organic material occurs at the interface, in particular, when a metal is vapor-deposited onto an organic material [7]. Due to the importance

[1] Author to whom any correspondence should be addressed.

of related effects in microelectronics and organic electronics, the diffusion and reaction of metal atoms in polymer films, as well as the dynamics of the metal film formation on top of polymers, have been studied in the past [8–16]. However, in organic electronic applications, the organic semiconductor is not necessarily a polymer, but can also be a (reactive) molecular solid [17].

Here, we consider especially the processes that occur when the metal electrodes are vapor-deposited onto the molecular organic materials under ultrahigh-vacuum conditions. Using a suitable model system that allows monitoring the diffusion depth of the metal, we study the extent of interlayer (interphase) formation. During the initial stages of metal deposition, single metal atoms impinge directly on the organic layer, where they can engage in the following processes: (a) desorption back into the gas phase [18, 19], (b) diffusion on the surface and (possibly) reaction with an organic molecule, (c) diffusion on the surface and attachment to a metal cluster, and (d) diffusion into the bulk and (possibly) reaction with a subsurface molecule or formation of (or attachment to) a subsurface metal cluster. Figure 1 illustrates these reaction pathways. Due to the low vapor pressure of most metals at room temperature, the supply of metal atoms into the subsurface region of the organic material is expected to stop as soon as there is a complete, closed metallic layer on top of the organic material [9]. Hence, the thickness of the interphase layer depends on the rate by which a complete metal film on the surface forms, relative to the rates of the competing processes, as long as the mobility of the molecules in the organic film is negligible and no molecular scrambling between reacted and unreacted molecules takes place. It should be emphasized that the formation of the closed metal film is the only limiting factor for the diffusion of the metal in the organic layer (unless there is a reaction and the reaction products create a barrier for diffusion). Without this self-limiting effect, the diffusion (and reaction) of the metal would likely continue indefinitely, creating a metalation reaction front that would propagate into the organic bulk material [20], creating a conceptually well understood instance of a reaction-diffusion system [20–26].

In this study, we attempt to influence the rate of formation of a closed metal film—relative to the rates of the competing processes—by changing various parameters: (a) temperature, (b) flux of metal atoms, and (c) chemical nature of the metal. These parameters should affect the interface formation as follows: (a) A lower temperature of the organic film during the metal deposition is expected to result in a lower diffusion rate of (thermalized) metal atoms on and in the film. Therefore, more metal atoms are expected to end up close to, or at, the surface. (b) Low metal-atom fluxes should be detrimental to the aggregation of the metal, because they reduce the probability of metal–metal encounters in favor of reactive encounters between metal atoms and molecules. It was previously shown by Faupel *et al* that flash deposition of metals onto polymers effectively reduces diffusion of the metals into the organic material [9]. (c) Chemical nature of the metal atom: A low reaction barrier facilitates the reaction between metal and molecules and thus the formation of the interphase. Conversely, the growth of a metal film as a competing process is impeded.

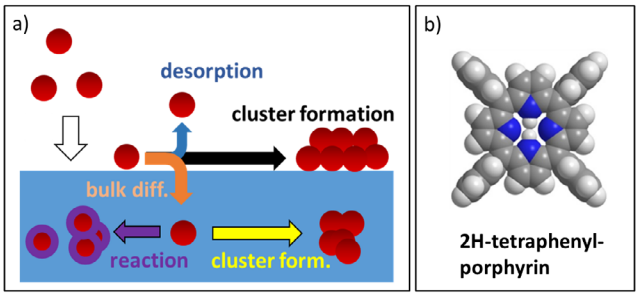

Figure 1. (a) Possible pathways for metal atoms upon vapor deposition onto a bulk phase of organic molecules. Metal atoms impinging on the surface can either desorb back into the gas phase, form cluster on the surface, or diffuse into the bulk, where they can again form (or attach to) clusters or react with the organic molecules. (b) The molecule used in this study: 2H-tetraphenylporphyrin (2HTPP).

We want to clarify how process parameters such as metal deposition rate, sample temperature, and chemical nature of the metal influence the interphase formation between an *in situ* deposited metallic layer and a bulk phase of organic molecules. For this aim, we use a bulk film of 2H-tetraphenylporphyrin (2HTPP) and study its reaction with vapor-deposited metallic Co and Fe. The interaction of 2HTPP with these metals is known to result in the formation of the respective M(II)tetraphenylporphyrins (MTPP, M = Co, Fe), according to the equation: $M + 2HTPP \rightarrow MTPP + H_2$ [27–29]. The MTPP interphase layer between the metal and the pristine 2HTPP is then investigated by chemical depth profiling with hard x-ray photoelectron spectroscopy (HAXPES). The porphyrin metalation represents a suitable model system for monitoring interfacial metal/organic reactions for several reasons. First, the reaction is well defined and typically does not have side reactions. Second, the pristine and the reacted organic material can easily be discriminated by x-ray photoelectron spectroscopy. Third, the metalation reaction works for a wide range of different metals [27, 28, 30]. According to previous work, the energy barrier for the metalation reaction of 2HTPP varies with the reactant metal. According to previous density functional theory (DFT) calculations, the reaction is barrierless in the case of Fe, while a small barrier of approximately 10 kJ mol^{-1} was predicted for Co [29]. This could lead to reactivity differences at the interface, particularly at low sample temperatures.

2. Experimental details

The samples were prepared *in situ* under ultrahigh voltage (UHV) conditions at the HIKE endstation of the KMC-1 beamline at BESSY II, Helmholtz-Zentrum Berlin [31, 32]. 2HTPP (98%, Porphyrin Systems) was evaporated at 660 K from a Knudsen cell and deposited onto a Si(0 0 1) surface and commercial Al foil. The deposition of 2HTPP, with typical fluxes of 2 nm min^{-1}, was monitored by a quartz crystal microbalance (QCM). Typical film thicknesses L were in the range of 40–60 nm.

Rods of cobalt (99.995%, Alfa Aesar) and iron (99.99+%, Hauner Metallische Werkstoffe) were used for metal vapor deposition using a commercial e-beam evaporator

Table 1. Material parameters and coefficients for 2HTPP, CoTPP, and FeTPP that are used for the calculation of the IMFP with equation (2).

Compound	Stoichiometry	H/C	Density ρ (g cm^{-3})	k_1	k_2	V_a (cm^3 mol^{-1})	Z^*
2HTPP	$C_{44}H_{30}N_4$	0.682	1.270	0.001 45	1	6.214	1.902
CoTPP	$CoC_{44}H_{28}N_4$	0.636	1.404	0.001 41	1	6.221	1.968
FeTPP	$FeC_{44}H_{28}N_4$	0.636	1.398	0.001 41	1	6.219	1.967

(FOCUS EFM-4). The metal deposition rates were either 0.7 nm min^{-1} or 0.035 nm min^{-1}, depending on the details of the experiment. During the deposition, a permanently mounted cold-cathode gauge indicated a pressure below 5×10^{-9} mbar. In subsequent x-ray photoelectron spectroscopy (XPS) experiments, no oxygen or other unwanted impurities were detected on the metallic films.

Photoelectron spectra were recorded close to normal emission (14° relative to the surface normal) with a VG Scienta R4000 electron spectrometer. A piece of gold foil, which was mounted in the analysis chamber of the HIKE endstation, was used to calibrate the binding energy scale with the Au $4f_{7/2}$ line at 84.0 eV. All HAXPES measurements were performed with the samples at room temperature, including those samples that had been cooled to 90 K during the metal deposition. In order to avoid beam damage during the measurements, the samples were systematically moved relative to the x-ray beam. The effectively irradiated area on the sample has dimensions of 0.2 mm × 4 mm (as measured in a calibration experiment); the elongated shape results from grazing incidence of the x-ray beam when the sample is in measurement position. The photon energy was varied between 3 keV and 5 keV; hereby, the Si(1 1 1) monochromator crystal was used for 3 keV and the Si(3 1 1) crystal for 5 keV photon energy. Changing the monochromator crystals allowed measuring the spectra with similar resolutions, irrespective of the photon energies [31, 32]. Although photon energies of up to 10 keV are available at this beamline, higher photon energies than 5 keV were not used because of the low cross sections, which lead to an increasingly unfavorable balance between signal-to-noise ratio on the one hand and radiation damage on the other hand. Moreover, photon energies below 2 keV, as available from, e.g. conventional AlKα or MgKα sources, are not suitable. With the resulting low information depths, the interphase region does not contribute sufficiently to the total XPS signal.

The acquired photoelectron spectra have been fitted with the following Pseudo-Voigt function [33, 34]:

$$\mathrm{PV} = (1-m)\sqrt{\frac{4\ln(2)}{\pi\,(\omega_{(x)})^2}}\exp\left(-\frac{4\ln(2)}{(\omega_{(x)})^2}\,x^2\right) + m\frac{1}{2\pi}\frac{\omega_{(x)}}{(\omega_{(x)}/2)^2+x^2}$$
$$\omega_{(x)} = \frac{2\,\omega_0}{1+\exp(-a(x-b))} \quad \text{where} \quad x = (E-E_0) \tag{1}$$

with the following parameters:

$\omega_{(x)}$	Full width at half maximum function	ω_0	Full width at half maximum parameter
a	asymmetry parameter, 0: symmetric peak	b	asymmetry shift parameter
E	binding energy	E_0	peak position

For background subtraction, a combination of Shirley background and second order polynomial has been used. The peaks and the background are displayed in the corresponding spectra.

The morphologies of the pristine 2HTPP layers were analyzed with atomic force microscopy (AFM, Nanoscope V, Bruker, USA). Topological imaging was conducted in tapping mode in air, using a sharp silicon nitride cantilever (SNL, tip radius 2 nm, spring constant $k = 0.24$ N m^{-1}, oscillation frequency $f = 56$–75 kHz).

3. Data analysis

In accordance with the results by Seah and Spencer [35], we will use the Gries G-1 equation [36, 37] to calculate the IMFPs in the investigated 2HTPP and MTPP/2HTPP layer systems (M = Co or Fe). In the G-1 equation, the inelastic mean free path (IMFP) λ is expressed as:

$$\lambda_{(E_{\mathrm{kin}})} = k_1\left(\frac{V_a}{Z^*}\right)\frac{E_{\mathrm{kin}}}{\log(E_{\mathrm{kin}}) - k_2}. \tag{2}$$

In this equation, the kinetic energy E_{kin} is given in eV and the IMFP λ in nanometers. For a certain compound, the parameter V_a is determined by the stoichiometry and density ρ of the material, while Z^* depends only on the stoichiometry [36]. The parameters k_1 and k_2 also depend on the material; for organic compounds, k_2 is unity and k_1 depends on the H/C ratio of the material: $k_1 = 0.0017$ at H/C = 1 and $k_2 = 0.0023$ at H/C = 2 [35, 36]. Seah and Spencer [35] found that a linear relation interpolation of k_1 for materials with H/C ratios different from either 1 or 2 leads to excellent results. Table 1 summarizes the parameters for 2HTPP, CoTPP, and FeTPP. V_a and Z^* are calculated according to Gries [36]. The density of the *in situ* prepared FeTPP was calculated under the assumption that its molar volume is identical to the air-stable and well characterized CoTPP.

The interphase formation was monitored by recording N 1s core level spectra at photon energies of 3 keV and 5 keV; the corresponding kinetic energies were 2.6 keV and 4.6 keV. These values result in the IMFPs given in table 2.

The N 1s signal intensity of the MTPP layer will be denoted as I_r (r for reacted) and the N 1s signal intensity of 2HTPP as I_{ur} (ur for unreacted). The intensities I_r and I_{ur} depend on the distribution of the reacted species within the near-surface region of the sample. For the mathematical treatment, it is helpful to think of the sample as a sequence of infinitesimally thin layers that are oriented parallel to the sample's surface at a distance z to the metal/MTPP interface. Each of these layers

Table 2. IMFPs for 2HTPP, CoTPP, and FeTPP for 3 and 5 keV photon energy obtained by application of equation (2).

Compound	$h\nu = 3$ keV (nm)	$h\nu = 5$ keV (nm)
2HTPP	5.10	8.18
CoTPP	4.80	7.70
FeTPP	4.80	7.70

consists of a fraction of metalated ($c_{r(z)}$) and unmetalated ($1 - c_{r(z)}$) molecules. Layers at a distance z to the interface contribute with a weight of $\exp(-z/(\mathrm{IMFP}\cos\theta))$ to the total signal (Beer–Lambert law, emission angle θ relative to the surface normal, IMFP: inelastic mean free path). Accordingly, the intensity ratio $I_r{:}I_{ur}$ can be expressed with the following equation:

$$\left(\frac{I_r}{I_{ur}}\right)_{(E_{kin})} = \frac{\int_0^L c_{r(z)}\ \exp(-z/(\Lambda_{(E_{kin},\,z)}\cos\theta))\mathrm{d}z}{\int_0^L (1 - c_{r(z)})\ \exp(-z/(\Lambda_{(E_{kin},\,z)}\cos\theta))\mathrm{d}z}. \tag{3}$$

Here, L stands for the total thickness of the organic layer, i.e. the initial thickness of the 2HTPP layer before metal deposition; θ is the photoelectron detection angle, in this study $\theta = 14°$. (Specifically in our experiments, L was chosen to be approximately 50 nm.) The effective IMFP, Λ, which is experienced by photoelectrons that emerge from a certain depth z, is given by the composition of the layers above; here, we estimate it as an average value of all IMFPs of the layers at depths between 0 and z:

$$\Lambda_{(E_{kin},\,z)} = \frac{1}{z}\int_0^z c_{r(z')}\,\lambda_{r(E_{kin})} + \left(1 - c_{r(z')}\right)\lambda_{ur(E_{kin})}\,\mathrm{d}z'. \tag{4}$$

The concentration profiles that are expected in our experiments are described with a *complementary error function* ('erfc'), a type of function that is frequently encountered in the analysis of concentration profiles in reaction-diffusion systems [20–26, 38–40] and theoretically predicted for this class of system [20]. Accordingly, the following equation was used to parameterize the curves (see figure 2(a)):

$$c_{r(z)} = 0.5 \cdot \mathrm{erfc}\left(\frac{z-d}{b}\right). \tag{5}$$

An individual concentration profile is described by two parameters: the 'width parameter' b and the 'reaction depth' d, see figure 2(a). (The width parameter is directly related to the width of the Gaussian function from which the error function is calculated.) It is of great importance in the discussion below that the integral of equation (5) is independent of the parameter b, as long as the reaction depth d is kept constant. For b close to zero, the curves approach the shape of a Heaviside step function. If one assumes such a strict layer-by-layer sequence of MTPP and 2HTPP, that is, an abrupt transition between a pure MTPP layer with a certain thickness d and a 2HTPP layer below, one can extract the value of d from the intensity ratio between the N 1s signals of MTPP and 2HTPP analytically. In this case, equations (3) and (4) lead to the following expression for $I_r{:}I_{ur}$, which is a transcendental equation for the reaction depth d:

$$\left(\frac{I_r}{I_{ur}}\right)_{(E_{kin})} = \frac{\lambda_{r(E_{kin})}}{\lambda_{ur(E_{kin})}} \times \frac{1 - \exp(-d/(\lambda_{r(E_{kin})}\cos\theta))}{\exp(-d/(\lambda_{ur(E_{kin})}\cos\theta)) - \exp(-L/(\lambda_{ur(E_{kin})}\cos\theta))}. \tag{6}$$

3.1. Limitations of the experimental approach

Before we proceed with the presentation and discussion of our results, an important question has to be addressed: is it possible to extract the shape of the concentration profile, and, in particular, the parameter b with arbitrary precision from HAXPES data? The samples in our study necessitate the use of hard x-rays to obtain sufficiently large values for the IMFP. Only in this way, signals originating from the buried metal/organic interface region contribute enough to the total signal. What are the consequences of the large IMFPs for our analysis?

In the limit of $\Lambda \to \infty$, the Beer–Lambert factor $\exp(-z/(\Lambda\cos\theta))$ in equation (3) is unity for all z, and, as a consequence, all concentration profiles with the same reaction depth d have the same intensity ratio $I_r{:}I_{ur}$, regardless of b. (This is due to the fundamental fact that the integral of the complementary error function is independent of the width parameter b.) A similar argument holds true for $\Lambda \gg b$: then, the Beer–Lambert factor $\exp(-z/(\Lambda\cos\theta))$ is practically constant in the region of interest $z = d \pm b$ where the erfc function changes from unity to zero. In this range for z, $\Lambda \gg b$ leads to:

$$\int \mathrm{erfc}\left(\frac{z-d}{b}\right)\exp\left(-\frac{z}{\Lambda\cos\theta}\right)\mathrm{d}z \approx \mathrm{const.}\int \mathrm{erfc}\left(\frac{z-d}{b}\right)\mathrm{d}z \tag{7}$$

where the last integral is independent of b. In other words, for $\Lambda \gg b$ the ratio $I_r{:}I_{ur}$ is only controlled by the reaction thickness d and not by the width parameter b.

We will demonstrate this numerical phenomenon with the data reported in a previous article by Chen *et al* [41] (see figure 2(b)). There, I_r and I_{ur} correspond, like in the present study, to the intensity ratios of metalated and unmetalated porphyrins. The authors use an equation equivalent to equation (6) (without distinguishing between different IMFPs for reacted and unreacted species), a fit by a genetic algorithm, and a SESSA simulation to show that the investigated system comprises a sharp layer-by-layer structure. Reproducing the procedures of Chen *et al* [41] (with additionally distinguishing between IMFPs for reacted and unreacted species, as well as using the complementary error function) we reach essentially the same result as these authors. However, we obtain further insight if we analyze the ensemble of concentration profiles that corresponds to an estimated confidence interval of the fit $I_r{:}I_{ur}$ (theory) versus $I_r{:}I_{ur}$ (experiment); this interval is highlighted as gray shaded region in figure 2(b). For the estimation, the width of the confidence band is calculated as two times the average deviation of the experimental data points from the best fit (black curve in figure 2(b)). We find that these concentration profiles cluster around a reaction depth of 1.55 nm, but show a wide variety of width parameters b, ranging from 0

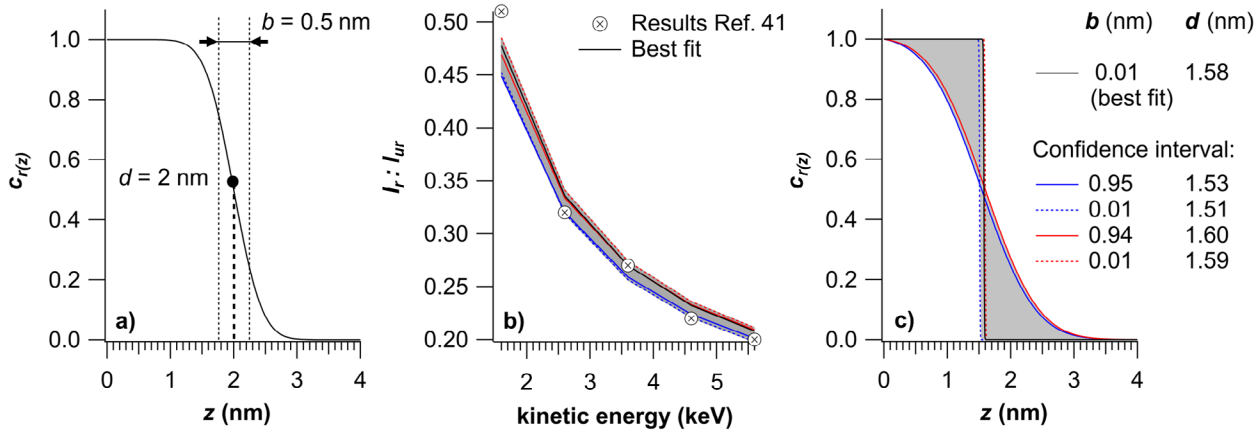

Figure 2. (a) A complementary error function for $b = 0.5$ nm and $d = 2$ nm. (b) Experimental I_r:I_{ur} values by Chen *et al* [41], along with the best fit to these data (black solid curve) and the estimated confidence region of the fit (gray shaded band). The width of the gray shaded band is two times the average deviation of the experimental data points from the best fit (black solid curve). It should be pointed out that the best fit, which gives an abrupt interface (black curve in frames (b) and (c)), has nearly exactly the same predicted I_r:I_{ur} values as a profile with high b (0.94 nm) and high d (1.6 nm) (solid red curve). (c) Range of different concentration profiles corresponding to the estimated confidence interval of the fit. The curves that define the 'envelope' of the ensemble are specifically highlighted in red and blue, and the associated I_r:I_{ur} values are highlighted in a similar way in (b).

to 0.95 nm. The gray shaded region in figure 2(c) contains all concentration profiles that are associated with the confidence interval in figure 2(b). In addition, the concentration profiles that define the 'envelope' of the ensemble in figure 2(c) are highlighted with red and blue color. Because the ensemble of possible concentration profiles includes (i) the abrupt layer-by-layer configuration ($b = 0$) and (ii) comprises concentration profiles with virtually identical reaction depths d, one can directly use equation (6) as a shortcut for calculating the reaction depth of this ensemble in a simple way.

We reach the following conclusion: the reaction depth d is a measure of the total amount of reacted molecules and can be extracted with high accuracy. However, an equally accurate extraction of the width parameter b (in the range of only a few Angstroms) would require an information depth Λ in the same order of magnitude as b, a condition that cannot be fulfilled because the examination of buried interfaces requires high IMFPs. As a consequence, we will only use the reaction depth d in the further discussion of our results, and stress the point that the actual shape of the concentration profile (i.e. the width parameter b) is not a reliable quantity under the specific experimental conditions in our experiments (i.e. large IMFPs in combination with typically small values for b).

4. Results and discussion

4.1. Morphology of the 2HTPP film

The morphology of the organic layer is an important factor that can potentially influence the metalation behavior and the morphology of the reaction zone (and of the resulting interphase layer) between the metal and the pristine 2HTPP. In a previous study [41], cobalt has been evaporated onto an 18 nm thick 2HTPP film supported on commercial aluminium foil; however, it was not clarified if this particular choice of film thickness and (relatively rough) carrier material is associated with (unwanted) morphological features of the 2HTPP layer.

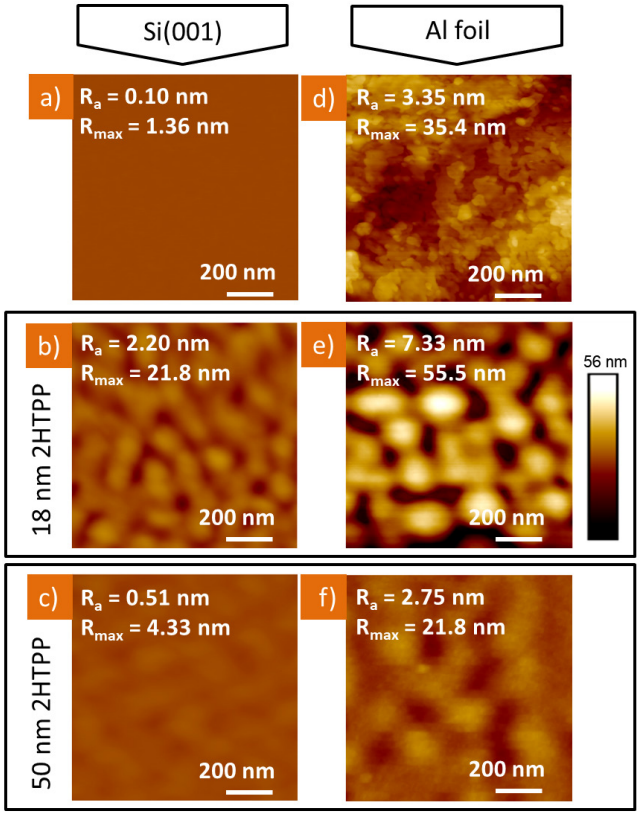

Figure 3. AFM images of the clean substrates (a) Si(0 0 1) and (d) Al foil, of 18 nm thick 2HTPP films on both substrates (b) and (e), and of 50 nm thick 2HTPP films on both substrates (c) and (f). The contrast in all images is normalized to the contrast in frame (e) to make all frames directly comparable; on this contrast scale, frame (a) does not show any features because of the very small roughness of the pristine Si(0 0 1) surface. R_a and R_{max} are the average and maximum roughness, respectively.

In order to determine the morphology of 2HTPP layers in the thickness regime $\leqslant$60 nm on a smooth substrate material, the molecules were vapor deposited onto a flat Si(0 0 1)

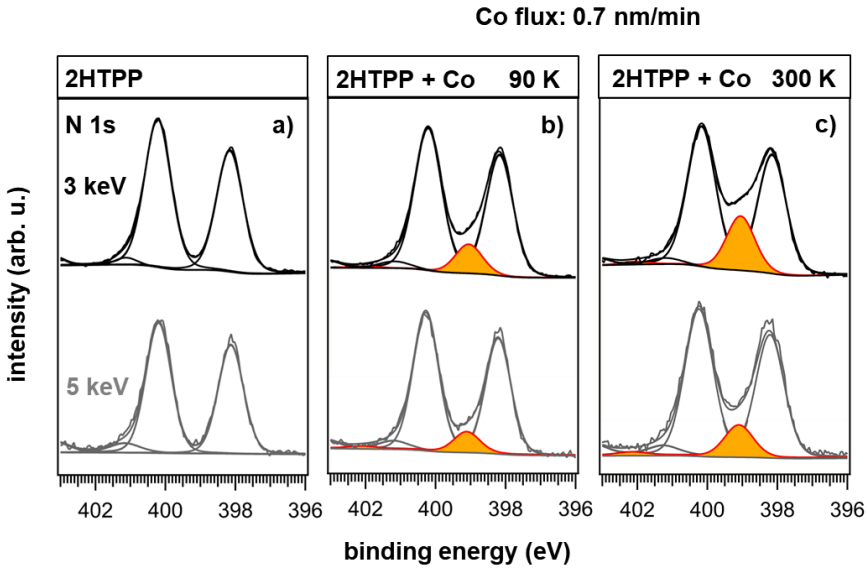

Figure 4. (a) N 1s XP spectra of a pristine 2HTPP layer (60 nm) on Si(0 0 1) taken at 3 and 5 keV photon energy. The two distinct peaks at 398.2 and 400.2 eV are attributed to iminic nitrogen (=N−) and pyrrolic nitrogen (−NH−), respectively. Additional peaks in the fit are satellites. (b), (c) After deposition of Co at 90 K (b) and 300 K (c), an additional peak emerges at 399.1 eV, which is attributed to the formation of CoTPP at the interface. Looking deeper into the material by increasing the photon energy from 3 to 5 keV reduces the relative contribution of this signal, indicating the formation of a CoTPP layer (as opposed to a homogeneous mixture of CoTPP and 2HTPP). When the 2HTPP film was held at 90 K during the deposition of Co, significantly less CoTPP is formed, compared to deposition at 300 K.

substrate with a very low average roughness R_a of 0.1 nm and maximum roughness R_{max} of 1.36 nm. (During deposition, the substrate was kept at room temperature.) The average roughness is defined as the variance of the height distribution on a given sample and is smaller than the maximum roughness, which can be observed by AFM. Large, smooth islands show a small average roughness but a high maximum roughness. After deposition of 18 nm 2HTPP, an increase in the roughness ($R_a = 2.20$ nm, $R_{max} = 21.8$ nm) was observed. The fact that the maximum height is larger than the nominal thickness is due to 3D island growth. Subsequent deposition of more material led to a reduction of the film roughness. At a 2HTPP film thickness of 50 nm, an average roughness of 0.51 nm and a maximum roughness of 4.33 nm were found.

In a reference experiment, Al-foil with an R_a value of 3.35 nm and R_{max} of 35.4 nm was used as a substrate to reproduce the conditions described in a previous publication [41]. As a result of the much higher roughness of the Al-foil, the deposited 2HTPP film were rougher on the Al-foil than on Si(0 0 1): After deposition of 18 nm 2HTPP onto Al-foil at 300 K, the sample showed a maximum roughness of 55.5 nm, compared to 21.8 nm for a 2HTPP film with the same thickness on Si(0 0 1). The nominally 18 nm thick 2HTPP film on Al foil (figure 3(e)) is not flat, but comprises large islands with heights in the range of 50 nm, at mutual distances of 100–200 nm. In this context, it is instructive to note that a spherical segment with a base diameter of 200 nm and a height of 45 nm contains the same volume as a flat, quadratic slab of material with 200 nm side length and 18 nm height. After deposition of further material, the roughness is reduced, reaching $R_a = 2.75$ nm and $R_{max} = 21.8$ nm at a film thickness of 50 nm. These values are significantly larger than those obtained with the Si substrate.

It appears that on both substrates, Al-foil and Si(0 0 1), thin multilayers (18 nm) consist of 3D islands, which merge together upon deposition of additional material, resulting in smoother films at higher thicknesses (50 nm). Because the 2HTPP films are more well defined on Si(0 0 1), this type of substrate was chosen for the HAXPES experiments that will be described in the following section.

4.2. Measurement of the reaction depths in M/MTPP/2HTPP systems

In order to examine the influence of different experimental parameters on the extension of the MTPP interphase layer between metals and 2HTPP, HAXPES measurements with photon energies of 3 and 5 keV were performed. These measurements were then used to calculate the reaction depths according to equation (6). The parameters of interest were: (i) the temperature of the organic film (90 and 300 K), (ii) metal flux (0.035 and 0.7 nm min^{-1}), and (iii) the chemical nature of the deposited metal (Fe and Co).

4.2.1. Temperature variation. In the first experiment, a cobalt film with a thickness of 4 nm (as measured by QCM) was deposited at a rate of 0.7 nm min^{-1} onto a 2HTPP film with a thickness of approximately 60 nm kept at 90 K during the deposition. The low temperature of the organic film during metal deposition was expected to reduce the rate of diffusion of metal atoms into the bulk. Likewise, the diffusion of CoTPP out of the reaction zone into the 2HTPP bulk should also be reduced. The related N 1s XP spectra, which were recorded at 3 and 5 keV photon energy, are shown in figure 4. For the pristine 2HTPP layer (figure 4(a)), two peaks at 398.2 eV (iminic nitrogen, =N−) and 400.2 eV (pyrrolic nitrogen, −NH−)

Table 3. Summary of the measured I_r:I_{ur} ratios and the resulting reaction depths. The values in brackets indicate the ±10% error interval of the ratio I_r:I_{ur}; the values in brackets, additionally highlighted in bold face, represent the associated values of d. For each experiment (that is, each column), 3 and 5 keV results for d are not significantly different from each other.

	Co, 90 K, 0.7 nm min^{-1}	Co, 300 K, 0.7 nm min^{-1}	Co, 90 K, 0.035 nm min^{-1}	Co, 300 K, 0.035 nm min^{-1}	Fe, 90 K, 0.7 nm min^{-1}	Fe, 300 K, 0.7 nm min^{-1}
3 keV	I_r:I_{ur} = 0.111 [0.099; 0.122]	I_r:I_{ur} = 0.210 [0.189; 0.231]	I_r:I_{ur} = 0.093 [0.084; 0.102]	I_r:I_{ur} = 0.211 [0.190; 0.232]	I_r:I_{ur} = 0.123 [0.111; 0.135]	I_r:I_{ur} = 0.211 [0.190; 0.232]
	d = 0.52 nm [0.47; 0.57]	**d = 0.95 [0.86; 1.03]**	**d = 0.44 [0.40; 0.48]**	**d = 0.95 [0.86; 1.04]**	**d = 0.58 [0.52; 0.63]**	**d = 0.95 [0.86; 1.04]**
5 keV	I_r:I_{ur} = 0.079 [0.071; 0.087]	I_r:I_{ur} = 0.118 [0.106; 0.130]	I_r:I_{ur} = 0.066 [0.059; 0.073]	I_r:I_{ur} = 0.138 [0.124; 0.152]	I_r:I_{ur} = 0.076 [0.068; 0.084]	I_r:I_{ur} = 0.125 [0.113; 0.138]
	d = 0.60 nm [0.54; 0.66]	**d = 0.88 [0.80; 0.97]**	**d = 0.51 [0.46; 0.55]**	**d = 1.02 [0.93; 1.12]**	**d = 0.58 [0.52; 0.63]**	**d = 0.93 [0.85; 1.02]**

are observed. After deposition of Co, an additional contribution appears at a binding energy of 399.1 eV (red line, yellow shading). This new contribution is associated with a metalloporphyrin complex, indicating that the central cavity of the porphyrin macrocycle incorporated a cobalt atom and released the −NH − hydrogen atoms as H_2, in line with previous work [28, 29, 42]. The relative intensities of the N 1s peaks associated with CoTPP (I_r) and 2HTPP (I_{ur}) (figure 4(b)) allow to estimate the width of the CoTPP layer. Increasing the photon energy from 3 keV to 5 keV, and consequently enhancing the IMFP for 2HTPP and CoTPP by a factor of approx. 1.6 (see table 2), leads to a smaller relative contribution of the N 1s signal from CoTPP: the ratio I_r:I_{ur} changes from 0.111 at 3 keV to 0.079 at 5 keV. This result is in agreement with the assumption of a layered system. (In contrast, in a homogeneous mixture of 2HTPP and CoTPP, the relative signal contributions would be independent of the degree of surface sensitivity of the individual measurements, i.e. they would be independent of the photon energy. This is apparently not the case here.) Using equation (6) with the above values for I_r:I_{ur}, we obtain reaction depths d of 0.52 nm and 0.60 nm for 3 keV and 5 keV, respectively. These thickness values are not significantly different from each other: If we assume a 10% experimental error of the ratio I_r:I_{ur} (estimated from the uncertainty in the actual shape of the signal background), we find that the corresponding error intervals for the thicknesses overlap. At 3 keV, the interval is 0.47 to 0.57 nm, and at 5 keV it is 0.54 to 0.66 nm. These intervals, plus the equivalent values for all following experiments, are compiled in table 3.

When the experiments were repeated with the 2HTPP film held at 300 K during metal deposition, a larger contribution of the reacted species (red line, yellow shading) was observed in the N 1s spectra (figure 4(c)), corresponding to a larger reaction depths d (i.e. a thicker CoTPP interphase layer). The related intensity ratios were I_r:I_{ur} = 0.210 and 0.118 at 3 and 5 keV, respectively. Again, this reduction of the I_r:I_{ur} ratio with increasing photon energy is a direct, but qualitative, indication for the presence of a distinct CoTPP layer. Application of equation (6) (with a 2HTPP layer thickness of 40 nm for this specific experiment) results in thicknesses of 0.95 nm (3 keV) and 0.88 nm (5 keV). Notably, the increase in temperature from 90 K to 300 K led to an increase in the width of the CoTPP layer by a factor of 1.6. Apparently, the mobility of 2HTPP and CoTPP is still low at 300 K—otherwise CoTPP and 2HTPP molecules would start to interdiffuse, which would lead to a transition away from a layered to a homogeneously mixed configuration. Hence, the increase in CoTPP layer thickness must be attributed to an increased mobility of the Co atoms after their adsorption on the surface.

4.2.2. Variation of the metal flux during deposition. In order to elucidate the influence of the metal flux on the extension of the CoTPP interphase, a further set of experiments with a reduced flux of 0.035 nm min^{-1} was conducted at sample temperatures of 90 K and 300 K. A lower flux of metal atoms reduces their transient concentration on the surface of the organic material. The thereby reduced probability for the encounter of the metal atoms is detrimental for the initial metal nucleation and cluster formation. The competing processes, i.e. the diffusion of the metal atoms into the organic film and the reaction with the molecules, should therefore be favored. This expectation is also in agreement with literature [8, 9].

Figure 5 shows the result for the deposition of Co at a reduced flux of 0.035 nm min^{-1} at 2HTPP film temperatures of 90 and 300 K. At 90 K (figure 5(a)), the differences to the experiments with a twenty-fold higher deposition rate are marginal. At 3 keV photon energy, the intensity ration I_r:I_{ur} is 0.093 and at 5 keV it is 0.066. With equation (6), this leads to thicknesses d of 0.44 nm (3 keV) and 0.51 nm (5 keV). The result is not significantly different from the corresponding low-temperature experiment with a Co flux of 0.7 nm min^{-1}. This unexpected result can be explained with the low temperature and the resulting small diffusion rate of Co, which confines the reaction to the topmost layer of the organic film, regardless of the flux.

Figure 5(b) shows the corresponding data for the low-flux Co deposition at 300 K. Here, the 3 keV measurement shows a ratio between reacted and unreacted signals of 0.211, while the measurement at 5 keV yields a ratio of 0.138. Application of equation (6) to these values results in reaction depths of 0.95 nm (3 keV) and 1.02 nm (5 keV). Again, this result is in contrast to the expectation: the flux reduction does not result in a significant increase of the reaction depth. Apparently,

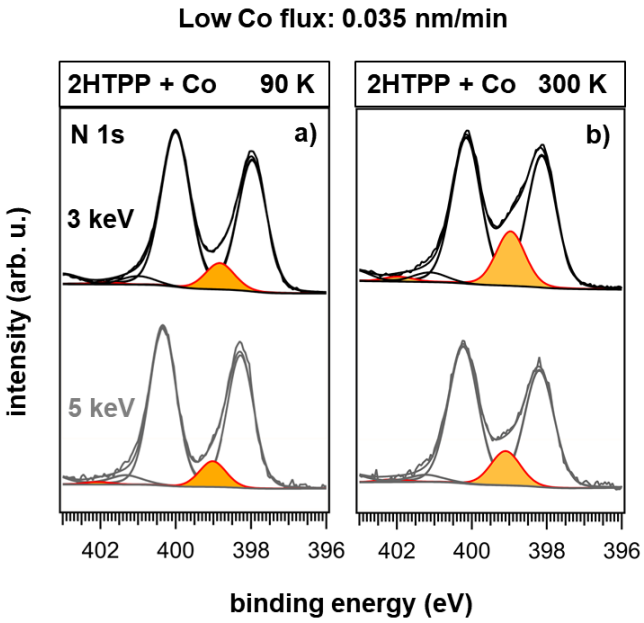

Figure 5. N 1s XP spectra of the Co/2HTPP reactive interface recorded with $h\nu = 3$ keV and 5 keV after cobalt deposition at a lower flux of 0.035 nm min^{-1}. Keeping the sample temperature at (a) 90 K results in a significantly thinner CoTPP layer than Co deposition at (b) 300 K.

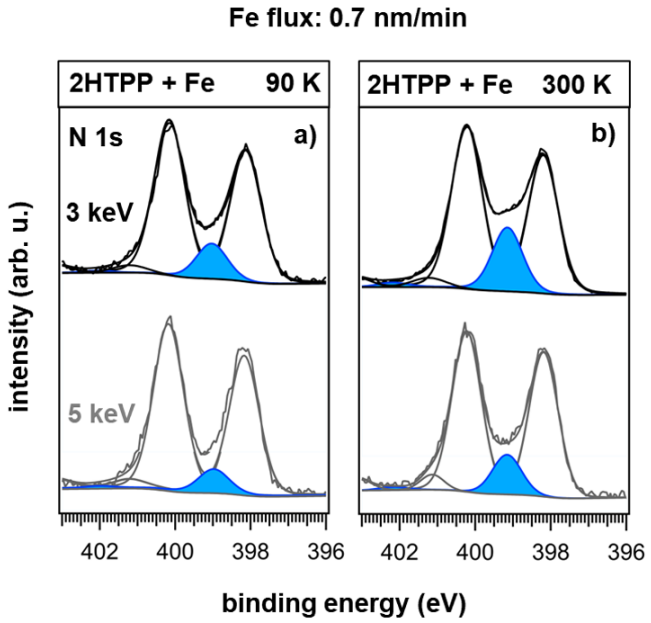

Figure 6. N 1s XP spectra recorded after iron deposition onto 2HTPP films with a flux of 0.7 nm min^{-1}. The photon energies were $h\nu = 3$ keV and 5 keV. At 90 K (a), the fraction of FeTPP (blue) is significantly smaller than at 300 K (b).

the variation of the flux by a factor of twenty is not enough to observe the anticipated effects. This result can possibly be attributed to attractive interactions between Co atoms and CoTPP molecules. These interactions could immobilize free cobalt atoms in the near-surface region even at room temperature and thus induce the initial formation of clusters on the organic film even at very low surface concentrations of metal atoms, i.e. at very low fluxes. (Note that only the initial metal nucleation and cluster formation are relevant here, because they depend on the surface concentration of the metal atoms. Once metal clusters are present on the surface, the relative probabilities for the attachment of a metal atom to a cluster versus its diffusion/reaction in the bulk becomes independent of the surface concentration of the metal atoms and, thus, independent of the flux of metal atoms. This follows from basic considerations of the reaction kinetics and the facts that both the cluster growth and the metalation reaction of the porphyrin are irreversible under the experimental conditions.) The formation of such a M—MTPP bond is not purely speculative, but is supported by DFT calculations from literature. For example, the bond between a Ag atom and a CoTPP molecule was found to have a dissociation energy of 92 kJ mol^{-1} [43]. That a bond of this strength can easily lead to the postulated trapping effect is shown by a simple estimation of the corresponding rate constant for bond dissociation: Assuming a pre-exponential factor of 1×10^{13} s^{-1}, the rate constant for the bond dissociation at 300 K is only 10^{-3} s^{-1}. This means that the average lifetime of a trapped metal atom is ~15 min. One way to test this hypothesis would be to extend the experiments to temperatures well above 300 K. However, this is not possible, because the elevated temperatures would lead to recrystallization of the organic films and thus make the (laterally integrating) HAXPES studies meaningless [44, 45]. The alternative approach, much lower metal fluxes, can also not be realized because of problems with sample contamination during the resulting extremely long deposition times.

4.2.3. Variation of the type of metal atoms. In a final set of experiments, iron was used instead of cobalt to clarify whether the surprisingly thin interphase layers observed in the Co/CoTPP/2HTPP system are specific for cobalt or also occur with other metals. It is known from (gas phase) DFT calculations that the reaction of 2HTPP with Co atoms has a small energy barrier of approximately 10 kJ mol^{-1}, while the porphyrin metalation reaction with iron proceeds without a barrier [29]. Thus, an increased amount of interface reaction may occur in the case of Fe deposition. In the first experiment, iron was deposited with a flux of 0.7 nm min^{-1} onto a 44 nm thick 2HTPP film, held at 90 K. Figure 6(a) shows the related N 1s HAXPES spectra. Measuring the intensity ratio I_r:I_{ur} results in values of 0.123 and 0.076 at 3 and 5 keV, respectively. These values are virtually identical to those observed for the deposition of Co under similar conditions (0.111 and 0.079). Hence, the calculated film thicknesses are 0.58 nm for both photon energies. Finally, when Fe was deposited with a rate of 0.7 nm min^{-1} onto a 42 nm thick 2HTPP film kept at 300 K (figure 6(b)), we found ratios of 0.211 (3 keV) and 0.125 (5 keV), leading to a thickness of 0.95 and 0.93 nm, respectively. It is not surprising that this experiment does not show significant deviation to the analogue Co experiment, because the differences between the metalation barriers for the different metals should not matter at room temperature. Table 3 summarizes the obtained ratios between reacted and unreacted species for the different systems.

The generally low reaction depths at low *and* ambient temperatures are even more surprising if one considers that metal atoms can usually easily diffuse through organic layers, unless special precautions are taken to prevent this movement [46]. For example, when gold was deposited onto a film of TMC-polycarbonate at 230 K with a rate of 0.1 nm min^{-1}, the metal was found to diffuse several tens of nanometers into the polymer [9]. In contrast, we find that Co and Fe atoms are exclusively present close to the surface of the porphyrin film. Apparently, there is a mechanism that traps the metal atoms efficiently in the near-surface region and allows only a few metal atoms to penetrate into the organic film before the metal film on top closes and disconnects the organic film irreversibly from further supply with single Co or Fe atoms. One candidate for such a mechanism is the M—MTPP interaction, which was theoretically predicted for related systems [43, 47]. It appears likely that the M—MTPP complexes, if they exist, would act as seeds for the growth of metal clusters, favoring a fast closure of the metallic film on top of the porphyrin layer. Similar effects are expected to occur in other reactive metal/organic interfaces when the reaction at the interface leads to the formation of metal complexes that can act as nucleation sites for the formation of metal clusters. The comparison of the investigated systems to the diffusion of gold atoms in polymers offers also another interesting aspect, regarding the different sizes of the metal atoms. Due to the fact that gold atoms are significantly larger than Co or Fe atoms, one would expect that the diffusion of gold atoms in organic materials is slower by several orders of magnitude—an effect that has indeed been observed in previous studies in inorganic samples [48, 49]. The fact that Fe and Co, despite their smaller atomic radii, show here much less diffusion than gold in an organic polymer further corroborates our conclusion that the free diffusion of Fe and Co is blocked by chemical interactions.

5. Summary

The formation of interlayers (interphases) at reactive metal-organic interfaces was studied with HAXPES. Specifically, it was shown that vapor deposition (under UHV conditions) of the transition metals iron and cobalt onto tetraphenylporphyrin (2HTPP) films leads to the formation of interlayers of the corresponding metalloporphyrins (CoTPP and FeTPP) between the metal and the pristine organic material. Variation of the deposition conditions revealed that the temperature of the organic material during the metal deposition is the single most important parameter that controls the thickness the MTPP interlayers. Deposition at 90 K resulted in FeTPP and CoTPP interphase layers that are roughly only half as thick as those obtained by room temperature deposition: typically ~0.5 nm at 90 K versus ~1 nm at 300 K. In contrast, variation of the metal flux within experimentally feasible boundaries (by a factor 20) had a negligible influence on the thickness of the formed MTPP interlayer. Likewise, very similar results were obtained for Fe and Co, despite differences in the reaction barriers for the formation of the respective metalloporphyrin complexes. The low values for the reaction depth generally indicate that metal diffusion into the 2HTPP film seems to be heavily restricted. Our results point towards the existence of a mechanism that traps the Co and Fe atoms close the 2HTPP film surface. In addition, we demonstrate that HAXPES readily provides the overall thickness of the formed interlayer, while the shape of the concentration profile at the MTPP/2HTPP interface cannot be reliably determined.

Acknowledgments

Financial support by the Deutsche Forschungsgemeinschaft (DFG) through the SFB 1083 ‘Structure and Dynamics of Internal Interfaces’ is gratefully acknowledged. We thank the Helmholtz-Zentrum Berlin for allocation of synchrotron radiation beamtime at BESSY II and financial support. Furthermore we want to express our gratitude to Dr Roberto Felix Duarte for assistance at the HIKE endstation. MS thanks the Stiftung Stipendien-Fonds des Verbandes der Chemischen Industrie for funding.

ORCID iDs

Martin Schmid https://orcid.org/0000-0002-1686-241X
Benedikt P Klein https://orcid.org/0000-0002-6205-8879
Nicolas Bock https://orcid.org/0000-0002-4990-8533

References

[1] Knupfer M and Peisert H 2005 Electronic properties of interfaces between model organic semiconductors and metals *Physics of Organic Semiconductors* ed W Brütting (New York: Wiley) p 41
[2] Koch N, Ueno N and Wee A T S (ed) 2013 *The Molecule-Metal Interface* (New York: Wiley)
[3] Scott J C 2003 *J. Vac. Sci. Technol.* A **21** 521
[4] Kumatani A, Li Y, Darmawan P, Minari T and Tsukagoshi K 2013 *Sci. Rep.* **3** 1026
[5] Tajima H, Yoshida K, Sato S, Kadoya T and Yamada J 2017 *J. Phys. Chem.* C **121** 14725
[6] Gao Y H, Shao Y D, Yan L J, Li H, Su Y T, Meng H and Wang X W 2016 *Adv. Funct. Mater.* **26** 4456
[7] Gottfried J M 2016 *New J. Phys.* **18** 111002
[8] Strunskus T, Kiene M, Willecke R, Thran A, von Bechtolsheim C and Faupel F 1998 *Mater. Corros.* **49** 180
[9] Strunskus T, Zaporojtchenko V, Behnke K, von Bechtolsheim C and Faupel F 2000 *Adv. Eng. Mater.* **2** 489
[10] Zaporojtchenko V, Strunskus T, Behnke K, Von Bechtolsheim C, Thran A and Faupel F 2000 *Microelectron. Eng.* **50** 465
[11] Leidheiser H and Deck P D 1988 *Science* **241** 1176
[12] Salaneck W R and Bredas J L 1996 *Adv. Mater.* **8** 48
[13] Ozawa K, Kakubo T, Shimizu K, Amino N, Mase K, Ikenaga E, Nakamura T, Kinoshita T and Oji H 2014 *Appl. Surf. Sci.* **320** 177
[14] Karim A and Kumar S (ed) 2000 *Polymer Surfaces, Interfaces and Thin Films* (Singapore: World Scientific)
[15] Sacher E, Pireaux J-J and Kowalczyk S P 1990 *Metallization of Polymers* (*ACS Symposium Series* vol 440) (Washington, DC: American Chemical Society)
[16] Sacher E (ed) 2002 *Metallization of Polymers* vol 2 (Dordrecht: Kluwer)

[17] Zhu X Y 2004 *Surf. Sci. Rep.* **56** 1
[18] Diaz S F, Zhu J F, Harris J J W, Goetsch P, Merte L R and Campbell C T 2005 *Surf. Sci.* **598** 22
[19] Zhu J F, Goetsch P, Ruzycki N and Campbell C T 2007 *J. Am. Chem. Soc.* **129** 6432
[20] Larralde H, Araujo M, Havlin S and Stanley H E 1992 *Phys. Rev.* A **46** R6121
[21] Fife P C and Ling H 1988 *Nonlinear Anal.* **12** 19
[22] Galfi L and Racz Z 1988 *Phys. Rev.* A **38** 3151
[23] Hilhorst D, vanderHout R and Peletier L A 1996 *J. Math. Anal. Appl.* **199** 349
[24] Langhoff T A and Schnack E 2008 *Chem. Eng. Sci.* **63** 3948
[25] Muntean A, Böhm M and Kropp J 2011 *Chem. Eng. Sci.* **66** 538
[26] Permikin D V and Zverev V S 2013 *Int. J. Heat Mass Transfer* **57** 215
[27] Diller K, Papageorgiou A C, Klappenberger F, Allegretti F, Barth J V and Auwärter W 2016 *Chem. Soc. Rev.* **45** 1629
[28] Marbach H 2015 *Acc. Chem. Res.* **48** 2649
[29] Shubina T E, Marbach H, Flechtner K, Kretschmann A, Jux N, Buchner F, Steinrück H P, Clark T and Gottfried J M 2007 *J. Am. Chem. Soc.* **129** 9476
[30] Gottfried J M 2015 *Surf. Sci. Rep.* **70** 259
[31] Gorgoi M *et al* 2009 *Nucl. Instrum. Methods Phys. Res.* A **601** 48
[32] Schäfers F, Mertin M and Gorgoi M 2007 *Rev. Sci. Instrum.* **78** 123102
[33] Schmid M, Steinrück H P and Gottfried J M 2015 *Surf. Interface Anal.* **47** 1080
[34] Schmid M, Steinrück H P and Gottfried J M 2014 *Surf. Interface Anal.* **46** 505
[35] Seah M P and Spencer S J 2011 *Surf. Interface Anal.* **43** 744
[36] Gries W H 1996 *Surf. Interface Anal.* **24** 38
[37] Werner W S M, Gries W H and Stori H 1991 *Surf. Interface Anal.* **17** 693
[38] Hagberg A and Meron E 1994 *Nonlinearity* **7** 805
[39] Batens N and Van Keer R 2003 *Chem. Eng. Sci.* **58** 4815
[40] Chopard B and Droz M 1991 *Europhys. Lett.* **15** 459
[41] Chen M, Zhou H, Klein B P, Zugermeier M, Krug C K, Drescher H J, Gorgoi M, Schmid M and Gottfried J M 2016 *Phys. Chem. Chem. Phys.* **18** 30643
[42] Gottfried J M and Marbach H 2009 *Z. Phys. Chem.* **223** 53
[43] Hieringer W, Flechtner K, Kretschmann A, Seufert K, Auwärter W, Barth J V, Görling A, Steinrück H P and Gottfried J M 2011 *J. Am. Chem. Soc.* **133** 6206
[44] Stöhr M, Gabriel M and Möller R 2002 *Europhys. Lett.* **59** 423
[45] Käfer D, Wöll C and Witte G 2009 *Appl. Phys. A: Mater. Sci. Process.* **95** 273
[46] Tai Y, Shaporenko A, Noda H, Grunze M and Zharnikov M 2005 *Adv. Mater.* **17** 1745
[47] Hötger D *et al* 2018 *Nanoscale* **10** 21116
[48] Dyson B F 1966 *J. Appl. Phys.* **37** 2375
[49] Hahn H and Averback R S 1988 *Phys. Rev.* B **37** 6533